J. Fluid Mech. (1999), *vol.* 395, *pp.* 211–236. Printed in the United Kingdom

Stability of non-parabolic flow in a flexible tube

By V. SHANKAR AND V. KUMARAN

Department of Chemical Engineering, Indian Institute of Science, Bangalore 560 012, India

(Received 11 November 1997 and in revised form 17 March 1999)

Flows with velocity profiles very different from the parabolic velocity profile can occur in the entrance region of a tube as well as in tubes with converging/diverging cross-sections. In this paper, asymptotic and numerical studies are undertaken to analyse the temporal stability of such 'non-parabolic' flows in a flexible tube in the limit of high Reynolds numbers. Two specific cases are considered: (i) developing flow in a flexible tube; (ii) flow in a slightly converging flexible tube. Though the mean velocity profile contains both axial and radial components, the flow is assumed to be locally parallel in the stability analysis. The fluid is Newtonian and incompressible, while the flexible wall is modelled as a viscoelastic solid. A high Reynolds number asymptotic analysis shows that the non-parabolic velocity profiles can become unstable in the inviscid limit. This inviscid instability is qualitatively different from that observed in previous studies on the stability of parabolic flow in a flexible tube, and from the instability of developing flow in a rigid tube. The results of the asymptotic analysis are extended numerically to the moderate Reynolds number regime. The numerical results reveal that the developing flow could be unstable at much lower Reynolds numbers than the parabolic flow, and hence this instability can be important in destabilizing the fluid flow through flexible tubes at moderate and high Reynolds number. For flow in a slightly converging tube, even small deviations from the parabolic profile are found to be sufficient for the present instability mechanism to be operative. The dominant non-parallel effects are incorporated using an asymptotic analysis, and this indicates that non-parallel effects do not significantly affect the neutral stability curves. The viscosity of the wall medium is found to have a stabilizing effect on this instability.

1. Introduction

Fluid flow in tubes with deformable walls is widely observed in biological systems and in industrial applications such as hollow fibre reactors and membrane bioreactors. Experimental evidence (Krindel & Silberberg 1979) suggests that the transition from laminar flow to turbulence in such systems could be very different from that of a rigid tube. In recent years, there has been renewed interest in the stability of fluid flow through flexible tubes (Kumaran 1995*a*, *b*, 1996, 1998*b*), and these studies have focused on the stability of the fully developed parabolic velocity profile. Flows with velocity distributions very different from the parabolic flow can occur in the entrance region of the tube prior to the formation of the fully developed flow. At moderate to high Reynolds number (Re), the length required for the flow development to occur is proportional to Re. The Reynolds number for the case of blood flow in the body varies from about 10^{-2} in capillaries to about 6000 in the large blood vessels (Lahav, Eliezer & Silberberg 1973; Silberberg 1987). Thus, there exists fluid flow in

flexible tubes where Re is of $O(10^3)$, and in these cases the length required for flow development will be quite large. In such situations, if the developing flow profiles in the flexible tube are more unstable than the parabolic profile, it is appropriate to base the critical Reynolds number for instability on the stability of the developing flow profile. In certain applications, the flexible tube may be converging slowly along the flow direction due to the applied pressure gradient; in such converging tubes, when $Re \gg 1$, the velocity profiles are very different from parabolic.

The objective of this paper is to develop asymptotic and numerical formulations to analyse the temporal stability of such 'non-parabolic' flows in a flexible tube. Kumaran (1996) generalized the classical theorems of hydrodynamic stability to inviscid flow in a flexible tube and predicted that the entrance flow velocity profile in a flexible tube and the flow in a slightly converging tube could become unstable in the inviscid limit. This instability is qualitatively different from the instabilities that have been observed in the earlier studies of Kumaran (1995*a*, 1998*b*), and from the instabilities observed in flow past compliant walls and compliant-walled channels. In this paper, relevant previous theoretical studies are discussed in § 2, and the method and results of this paper are compared with those of earlier studies in § 3. An asymptotic analysis of the stability equations in the $Re \gg 1$ limit is carried out in § 4, and a numerical solution of the governing equations is presented in § 5. Results from the numerical solution are discussed in § 6. Our asymptotic results show that the non-parabolic velocity profiles of interest are indeed unstable in the $Re \to \infty$ limit, thus verifying the prediction of Kumaran (1996). Numerical results reveal that the non-parabolic flows can be unstable at much lower Reynolds number than the parabolic flow, and this instability can be important in the transition in fluid flow through flexible tubes. The stability of the non-parabolic profiles is first determined using the parallel flow approximation, where the gradient of the mean flow in the axial direction and the radial component of the mean flow are neglected. This is a good approximation in the $Re \gg 1$ limit, because the length scale for the variation of the mean velocity is $O(Re)$ larger than the radius of the tube. The error incurred due to the parallel flow approximation is estimated using an asymptotic analysis in § 7, where the largest correction to the stability equations due to the axial gradient of the mean velocity is included, and the change in the neutral curves due to this correction is calculated. A summary of the important conclusions of this paper is given in § 8.

2. Previous theoretical studies

In this section, we review the instabilities that have been observed in flow past compliant walls and compliant-walled channels. The earlier classification of instabilities in flow past flexible walls by Benjamin (1960) and Landahl (1962) was based on the effect of wall dissipation on the stability of the modes, while the classification of Carpenter & Garrad (1985, 1986) was based on the absence of these modes in flow past rigid surfaces. These classifications are inadequate because there are many modes of instability in flexible channels and tubes that could share similar qualitative features according to the previous classification, but where the mechanism of instability could be very different. Consequently, it is more appropriate to classify the instabilities according to the following criteria : (i) asymptotic behaviour of the modes at the high/low Reynolds number limit and high/low wavelength limit, (ii) the flow structure of the unstable modes (e.g. the thickness of the boundary layer), (iii) the mechanism of instability, and (iv) the specific features of the wall dynamics for which these modes are observed. According to these characteristics, we classify below the

instabilities analysed in the earlier studies on flows in flexible channels/tubes and flow past compliant surfaces. This classification makes evident the qualitative differences between the instability analysed in this paper from that of earlier studies, and it places the present work in perspective.

(A) *Viscous instability*

This instability is observed in wall materials of finite thickness with shear modulus G which are described by linear elasticity equations for the displacement field in the material in the low Reynolds number regime where $Re \ll 1$ and $(V\eta/(GR)) \sim O(1)$. Here, ρ and η are the density and viscosity of the fluid, R is the radius of the tube, V is the characteristic fluid velocity and G is the shear modulus of the wall medium. The viscous modes become unstable when the fluid velocity is increased beyond a critical value even in the absence of fluid inertia. The mechanism of instability is the transfer of energy from the mean flow to the perturbations due to the shear work done by the mean flow at the interface between the fluid and the wall medium. In the limit of $Re \to 0$ the scaling relation between Re and the quantity $\Sigma \equiv \rho GR^2/\eta^2$ turns out to be $Re \sim \Sigma$. Viscous modes were first studied by Kumaran, Fredrickson & Pincus (1994) for Couette flow past a flexible surface, and this was extended by Kumaran (1995*a*) to the stability of Hagen–Poiseuille flow in a flexible tube. The continuation (Kumaran 1998*b*; Srivatsan & Kumaran 1997) of the viscous modes to the intermediate-Re regime revealed that at high Re, the scaling relation becomes $Re \sim \Sigma^{\alpha}$, where α takes a value between 0.7 and 0.75.

(B) *Low Reynolds number long-wave instability*

This instability has been found for flow past spring-backed plates and membranes. These modes are neutrally stable in the viscous limit $Re \to 0$. However, the inertial correction to the governing equations in the limit of low wavenumber (k) destabilizes these modes, and the destabilizing mechanism is the transfer of energy due to the inertial terms in the conservation equation in the limit $k \to 0$. This type of instability was predicted in the analysis of Kumaran & Srivatsan (1998) for the case of Couette flow past a membrane, and by LaRose & Grotberg (1997) for the developing flow through a channel with spring-backed walls. A continuation of this type of instability to finite k and Re was carried out by LaRose & Grotberg (1997) and Kumaran & Srivatsan (1998). LaRose & Grotberg (1997) classify two types of instability depending on the wavenumber at which the transition Reynolds number is a minimum. When the transition first occurs at $k \to 0$, the instability is called a 'long-wave instability' while the instability is termed a 'flutter' instability if the transition first occurs at a finite value of k. However, both of these are continuations of the same solutions obtained from the $k \ll 1$ limit where the inertial terms are neglected in the leading approximation, and the physical mechanism of these instabilities is the same.

(C) *Rigid surface modes*

These modes exist in the flow past rigid surfaces, but in flow past flexible surfaces they are modified by wall flexibility. The neutral stability curve has a characteristic lower and upper branch in the (Re, k)-plane, and Re scales as $k^{-1/8}$ in the lower branch of the neutral curve in the limit of high Re. The mechanism of instability is the work done by the Reynolds stresses in a critical layer of thickness $Re^{-1/3}$ in the flow, where the viscous forces become important. There have been many studies on the effect of wall flexibility on the Tollmien–Schlichting instability for the flow past a wall made of spring-backed plates, for example the classic paper of Benjamin (1960),

Carpenter & Garrad (1985), Carpenter & Gajjar (1990), Davies & Carpenter (1997). For parabolic flow through a flexible tube with an elastic wall of finite thickness, the study of Kumaran (1998*b*) has recovered the stable solutions of axisymmetric perturbations in a rigid tube in the limit $G/\rho V^2 \gg 1$. Kumaran (1998*c*) has recovered the stable wall modes in a rigid tube. In this paper, we recover the neutral modes of Garg (1981) for the stability of the developing flow in a rigid tube in the limit of large wall elasticity.

(D) *Regular inviscid modes*

These are observed in the limit $Re \gg 1$ and $\rho V^2/G \sim O(1)$, and they do not exist in the flow past rigid surfaces. In the limit of high Re, the flow is inviscid in the core of the tube, and there is a wall layer of thickness $O(Re^{-1/2})$ smaller than the tube radius where the viscous stresses are $O(Re^{-1/2})$ smaller than the inertial stresses. The destabilizing mechanism in this case is the work done by the pressure forces on the wall material. This type of instability has been observed in flows past walls made of spring-backed plates. The instability observed in Carpenter & Garrad (1986), which is a Kelvin–Helmholtz-type instability where the discontinuity of the mean velocity profile at the interface is the driving force, belongs to this category. Asymptotic and numerical studies of regular inviscid modes have also been carried out by Carpenter & Gajjar (1990) for a Blasius boundary layer past a compliant wall and Davies & Carpenter (1997) for fully developed flow in a two-dimensional channel with compliant walls. Regular inviscid modes were analysed by Kumaran (1995*b*) for a parabolic profile, and in this paper for non-parabolic velocity profiles in flexible tubes with walls of finite thickness made of a viscoelastic material. Both these studies used an asymptotic analysis in the small parameter $Re^{-1/2}$ and, in contrast to the previous studies mentioned above, these analyses revealed that regular inviscid modes are *stable* for the velocity profiles considered in these studies.

(E) *Singular inviscid modes*

For non-parabolic flows in a flexible tube, in the $Re \to \infty$ limit, the leading-order inviscid stability equation contains a singularity where the wave speed of the disturbances equals the local fluid velocity. This singularity is absent in the stability of parabolic flows to axisymmetric disturbances, and this qualitatively modifies the nature of the instability. The flow structure near the singular point is similar to that near a critical layer in the flow past rigid surfaces, and the mechanism of instability is the work done by the Reynolds stresses in the critical layer. However, there are important differences between these and rigid surface modes. The critical Re scales as $Re \sim \Sigma^{1/2}$ in the limit $\Sigma \gg 1$ (where the non-dimensional parameter Σ is proportional to the shear modulus of the wall medium), in contrast to the rigid surface instability (Type C in this classification) where the critical Re approaches the finite value appropriate to that for flow past a rigid surface in the limit $\Sigma \gg 1$. Consequently, this mode of instability does not exist in a rigid tube. In addition, the shape of the neutral stability curve in the (Re,k)-plane is very different from that in the flow past rigid surfaces. For the singular inviscid modes, $Re \sim k^{-1}$ in the limit $k \ll 1$, has a minimum at a finite value of k and $Re \sim k$ in the limit $k \gg 1$ (see the Appendix). The instability analysed in this paper belongs to this class of modes.

(F) *High Reynolds number wall modes*

For these modes, the vorticity is confined to a layer of thickness $O(Re^{-1/3})$ at the wall. These are distinct from the inviscid modes where the vorticity is confined to a

region of thickness $O(Re^{-1/2})$. Wall modes are stable for flow in a rigid tube, but the wall flexibility modifies these modes in a flexible tube. A scaling analysis (Kumaran 1998*a*) indicates that the elastic stresses in the wall affect the damping of the wall modes when the dimensionless number $\Lambda \equiv Re^{1/3}(G/\rho V^2)^{1/2} \sim O(1)$, and in this regime the elastic stress is large compared to the inertial stress in the wall material. This analysis shows that there is one mode in a flexible tube whose growth rate does not converge to any of the rigid tube modes, but which has a diverging frequency in the limit $\Lambda \to \infty$. This is the least-stable wall mode in a flexible tube. This least-stable wall mode was continued numerically Kumaran (1998*c*) to the $\Lambda \ll 1$ regime, and it was observed that this mode becomes unstable when Λ is decreased below a transition value at a fixed Re. In this case, the critical Reynolds number scales as $Re \sim \Sigma^{\alpha}$ where α is between 0.7 and 0.75.

From the above classification, it is clear that the singular inviscid modes analysed in this paper are qualitatively different from the modes analysed in earlier studies. Our asymptotic analysis is also different from that carried out in earlier studies on rigid tubes and spring-backed plates, and it is useful to examine the differences. The non-parallel analysis of Smith & Bodonyi (1980) for stability of the developing flow in a rigid tube assumes the scaling $Re \propto k^{-1/8}$ in the limit $k \to 0$ along the lower branch of the neutral curve obtained from the parallel flow stability theory. In a similar fashion, Carpenter & Gajjar (1990) and Davies & Carpenter (1997) assume that $Re \gg 1$, so that viscous effects are negligible, and consider $k \to 0$ so that only the leading-order terms in a low-wave-number expansion are included. The analysis of LaRose & Grotberg (1997) is a little different, because they assume that $k \to 0$, and neglect the inertial terms in the leading approximation. However, in all these studies the limit $k \to 0$ is assumed in the asymptotic analysis. In contrast, in our asymptotic analysis only the limit $Re \gg 1$ is assumed, and the wavenumber is an $O(1)$ quantity. The scaling information of the type used by Smith & Bodonyi (1980) for the parallel flow stability is not available for the present system, and it is first necessary to determine the stability using the parallel flow approximation. Moreover, the primary interest in our study is the critical Reynolds number, which is the lowest Reynolds number for which neutrally stable modes exist. The wavenumber corresponding to the critical Reynolds number is $O(1)$ in this paper. Consequently, in our non-parallel analysis the limit $k \ll 1$ is not assumed and we determine the largest corrections due to non-parallel effects for the most unstable modes which have $k \sim O(1)$.

3. Problem formulation and governing equations

The system consists of a Newtonian, incompressible fluid of density ρ and viscosity η flowing in a tube of radius R surrounded by a viscoelastic medium in the region $R < r < HR$. In the limit of high Reynolds number, the lengths are scaled by the tube radius R, the time by $(\rho R^2/G)^{1/2}$ and all velocities by $(G/\rho)^{1/2}$. The scaled Navier–Stokes mass and momentum equations for the fluid are

$$\partial_l v_l = 0, \tag{3.1}$$

$$\partial_t v_l + v_j \partial_j v_l = -\partial_l p_f + \epsilon \Gamma \, \partial_j^2 v_l. \tag{3.2}$$

In both these equations and in what follows, repeated indices imply a summation over the index unless stated otherwise. Here, $\partial_t = (\partial/\partial t)$ and $\partial_l = (\partial/\partial x_l)$, $\epsilon = 1/Re$, and Re is the Reynolds number defined as $Re = \rho \overline{V} R/\eta$ where $\overline{V}$ is the average velocity of the basic laminar flow. The parameter Γ is the non-dimensional average

velocity of the basic laminar flow and is given by $\Gamma = (\rho \overline{V}^2/G)^{1/2}$. The fluid pressure p_f is non-dimensionalized by the shear modulus G in (3.2). The stresses in the fluid are given by

$$\tau_{lj} = -p_f \delta_{lj} + \epsilon \Gamma (\partial_l v_j + \partial_j v_l). \tag{3.3}$$

The flexible wall is modelled as a viscoelastic solid continuum, and the dynamics of the wall motion is described by the governing equations for an incompressible elastic material modified to include viscous stresses (Kumaran 1995*a*, *b*, 1998*b*). The wall dynamics is described by a displacement field u_l which characterizes the displacement of the material points of the wall from their steady-state positions due to fluid stresses at the interface. In what follows, the subscript g in a quantity implies that it is a property of the wall medium. The incompressibility condition requires that

$$\partial_l u_l = 0. \tag{3.4}$$

The momentum balance equation for the wall medium is given by

$$\partial_t^2 u_l = -\partial_l p_g + \partial_j^2 u_l + \epsilon \Gamma \eta_r \partial_j^2 v_l. \tag{3.5}$$

The left-hand side of the above equation describes the rate of change of momentum in a volume element in the wall medium and the three terms on the right-hand side of the equation are, respectively, the gradient of the pressure, the divergence of an elastic stress due to the strain in the wall and the divergence of a viscous stress due to the strain rate. Here, $v_l = \partial_t u_l$ is the velocity field at the wall and $\eta_r = \eta_g/\eta$ is the ratio of wall to fluid viscosity. The stress in the wall medium is given by

$$\sigma_{lj} = -p_g \delta_{lj} + (\partial_l u_j + \partial_j u_l) + \epsilon \Gamma \eta_r (\partial_l v_j + \partial_j v_l). \tag{3.6}$$

The boundary conditions for the fluid velocity field v_l are the symmetry conditions at the centre of the tube, namely $v_r = 0$ and $\partial_r v_x = 0$. The viscoelastic material is fixed to a rigid support at $r = H$ where the displacement field satisfies $u_r = 0$ and $u_x = 0$. At the interface between the fluid and the wall, the velocity and stress are continuous:

$$v_l = \partial_t u_l, \quad \sigma_{lj} = \tau_{lj}. \tag{3.7}$$

The base flows whose stability is of interest here are (i) the developing flow velocity profile for fluid flow in a tube, and (ii) the flow in a slightly converging tube. In non-dimensional form, the base flow is represented as

$$\bar{v}_x = \Gamma U(r, x), \qquad \bar{v}_r = Re^{-1} \Gamma V(r, x). \tag{3.8}$$

The length required for the flow to develop to 95% of the fully developed state is given by $0.13RRe$, where $Re = R\overline{V}\rho/\eta$, and R is the radius of the tube (Tritton 1977; Duncan, Thom & Young 1960). Since the length scale for flow development is of $O(Re)$, the radial component of the mean velocity ($\bar{v}_r$) is of $O(Re^{-1})$ less than the axial component of the mean velocity. In (3.8) $U(r, x)$ and $V(r, x)$ are respectively the non-dimensional functional form of the axial and radial velocity profiles of the base flow. For a fully developed parabolic Poiseuille flow, $U(r, x) = 2(1 - r^2)$ and $V(r, x) = 0$.

In a developing flow, $U(r, x)$ depends on both r and x and this functional form is determined numerically by solving the appropriate Navier–Stokes equations. In this paper, as in the stability analysis of Garg (1981), the mean velocity profiles $U(r, x)$ were obtained using the method of Hornbeck (1963), and our results are in excellent agreement with the data provided in Garg (1981) and Hornbeck (1963). The second type of mean velocity profile analysed here is that in a 'slightly converging tube', where

the angle between the tube wall and the axial direction $\alpha \ll 1$ and the product $\alpha Re \sim 1$. A similar limit was considered in the papers of Eagles & Weissman (1975) and Eagles & Smith (1980) where the stability of slowly varying two-dimensional rigid channels was considered. This parameter regime is of interest for the following reason. For a steady unidirectional flow in a cylindrical tube, the inertial terms in the momentum equations are identically zero. However, if there is a slight taper of angle α in the walls of the tube, the ratio of the inertial and viscous terms in the momentum equation is $O(\alpha Re)$. When $Re \gg 1$, this ratio could be $O(1)$ even though the taper (α) is small, and the velocity profile could be significantly different from the parabolic velocity profile due to the effect of the inertial terms. The velocity profile in the converging tube depends on the initial velocity profile at the inlet. Our computations show that a plug velocity profile at the inlet resulted in velocity profiles that are qualitatively similar to that for the developing flow in a straight circular tube. Consequently, the instability that is observed for the developing flow velocity profile would be observed in a converging tube as well. Hence, we chose a parabolic distribution at the inlet of the converging tube. In a converging tube, a fully developed state cannot occur and the parabolic flow at the inlet becomes progressively non-parabolic as one proceeds downstream. The converging tube velocity profiles computed in this work were found to be in good agreement with the finite difference results of Sutterby (1965).

The stability analyses of spatially developing flows in the $Re \gg 1$ limit usually invoke the 'parallel flow' assumption, and neglect the axial gradients in the mean velocity and the radial component of the mean velocity. According to the parallel flow assumption, the mean flow is considered to be unidirectional

$$\bar{v}_x = U(r, x) \approx U(r) \text{ and } \bar{v}_r = 0, \tag{3.9}$$

where the mean velocity $U(r, x)$ is determined from the solution of the Navier–Stokes equations for the base flow at the axial position x. The error made due to the parallel flow assumption is examined using an asymptotic analysis in § 7. This approximation permits the use of the classical normal mode analysis. Small axisymmetric perturbations in the form of Fourier modes are imposed on the fluid velocity field and the wall displacement field as follows:

$$v_i = \tilde{v}_i \exp(\mathrm{i}k(x - ct)), \quad u_i = \tilde{u}_i \exp(\mathrm{i}k(x - ct)). \tag{3.10}$$

Here, k, the wavenumber of perturbations is real, the wave speed c ($= c_r + \mathrm{i}c_i$) is complex and perturbations are unstable for $c_i > 0$. The above form for perturbations is inserted into the governing equations for the fluid velocity field to obtain the following Orr–Sommerfeld (OS)-type fourth-order ordinary differential equation for $\tilde{v}_r$:

$$(\Gamma U - c)(\mathrm{d}_r^2 + r^{-1}\mathrm{d}_r - r^{-2} - k^2)\tilde{v}_r - \Gamma(U'' - r^{-1}U')\tilde{v}_r = \frac{\Gamma}{\mathrm{i}kRe}(\mathrm{d}_r^2 + r^{-1}\mathrm{d}_r - r^{-2} - k^2)^2\tilde{v}_r. \tag{3.11}$$

Here and in what follows, $\mathrm{d}_r = \mathrm{d}/\mathrm{d}r$, and a prime indicates differentiation with respect to r. The linearized equation for the displacement field in the wall medium can be obtained in a similar manner by inserting the expressions for the perturbation to the displacement field (3.10) into the governing equations for the wall medium (3.4) and (3.5) to obtain a single fourth-order differential equation for u_r:

$$[(1 - \mathrm{i}kc\epsilon\Gamma\eta_r)(\mathrm{d}_r^2 + r^{-1}\mathrm{d}_r - r^{-2} - k^2) + k^2c^2](\mathrm{d}_r^2 + r^{-1}\mathrm{d}_r - r^{-2} - k^2)\tilde{u}_r = 0. \tag{3.12}$$

The boundary conditions for the fluid are the two symmetry conditions at the centre

of the tube $r = 0$, $\tilde{v}_r = 0$, $\mathrm{d}_r\tilde{v}_x = 0$. The boundary conditions for the viscoelastic medium are the zero displacement conditions at $r = H$, $\tilde{u}_r = 0$ and $\tilde{u}_x = 0$. The boundary conditions at the interface between the fluid and the wall are the continuity of velocities and stresses applied at the perturbed interface. These are expanded in a Taylor series about their values at the undisturbed interface $r = 1$, and the linear terms retained, to obtain the following conditions at $r = 1$:

$$\left.\begin{aligned} &\tilde{v}_r = -\mathrm{i}kc\tilde{u}_r,\ \ \tilde{v}_x + \mathrm{d}_r\bar{v}_x|_{r=1}\,\tilde{u}_r = -\mathrm{i}kc\tilde{u}_x, \\ &\tilde{\tau}_{rr} = \tilde{\sigma}_{rr},\ \ \mathrm{d}_r\bar{\tau}_{xr}|_{r=1}\,\tilde{u}_r + \tilde{\tau}_{xr} = \mathrm{d}_r\bar{\sigma}_{xr}|_{r=1}\,\tilde{u}_r + \tilde{\sigma}_{xr}. \end{aligned}\right\} \tag{3.13}$$

The second term in the left side of the tangential velocity condition ($\mathrm{d}_r\bar{v}_x|_{r=1}\tilde{u}_r$) has a term proportional to $\tilde{u}_r$ and this represents the variation in the mean velocity at the surface due to the displacement at the surface (Kumaran 1995*a*, *b*). There is a discontinuity in the first derivative of the tangential stress at the fluid–wall interface in the base state, and this is reflected in the tangential stress boundary condition. For the special case of parabolic flow in a flexible tube, the first derivative of tangential stress is continuous at the fluid–wall interface, and thus this term was not present in the analysis of Kumaran (1995*a*, *b*). The variation in the normal stresses across the interface is of $O(Re^{-1})$, and this term is neglected in the parallel flow approximation. The two fourth-order differential equations (3.11) and (3.12) along with eight boundary conditions (two at $r = 0$, two at $r = H$ and four at $r = 1$ (3.13)) constitute an eigenvalue problem for c for given values of Γ, k and Re. The eigenvalue problem yields a highly nonlinear equation for c, and it is necessary to have a good initial guess to obtain solutions to this equation. This is provided by an asymptotic analysis of the governing equations in the limit of high Reynolds number in the next section.

4. High Reynolds number limit

For $Re \gg 1$, the viscous terms in the OS-like equation (3.11) are $O(\epsilon)$ smaller than the inertial terms, where $\epsilon = Re^{-1}$. An asymptotic analysis in the small parameter ϵ is suitable, and the leading-order inviscid stability equation, which is obtained by neglecting the viscous terms in (3.11), is the axisymmetric counterpart of the Rayleigh equation:

$$(\mathrm{d}_r^2 + r^{-1}\mathrm{d}_r - r^{-2} - k^2)\tilde{v}_r - \frac{\Gamma(U'' - r^{-1}U')}{(\Gamma U - c)}\tilde{v}_r = 0. \tag{4.1}$$

There are two different classes of neutrally stable modes for $\tilde{v}_r(r)$ depending on the magnitude of c, when c is real ($c_i = 0$) (see Chap. 4 of Drazin & Reid 1981). If $c_r > \max(\Gamma U)$, the solutions of the differential equation are regular for all r in the range $0 < r < 1$, and this class of solutions is classified as 'regular inviscid modes'. However, if c_r is in the range $0 < c_r < \max(\Gamma U)$, and if $(U'' - r^{-1}U') \neq 0$, (this is usually the case for non-parabolic velocity profiles) the point where $c_r = U$ is a regular singular point of the differential equation and $\tilde{v}_r(r)$ is a singular neutral solution. The point at which $\Gamma U = c$ is called the critical point, r_c, and the region around r_c is referred to as the 'critical layer', and neutrally stable modes having a critical layer are called 'singular inviscid modes'. For parabolic flows, there are no singular neutral modes because $(U'' - r^{-1}U') = 0$ (Kumaran 1995*b*), but in non-parabolic flows there could be both regular and singular neutral modes.

4.1. *Analysis of regular inviscid modes*

For these modes, the leading-order inviscid stability equation (4.1) is regular for $0 \leqslant r \leqslant 1$, and an analysis similar to that of Kumaran (1995*b*) is suitable. The fluid velocity field can be divided into two regions – an outer region with velocity $\tilde{v}_{oi}$ and a wall layer with velocity $\tilde{v}_{wi}$ where the viscous effects are important: $\tilde{v}_i = \tilde{v}_{oi} + \tilde{v}_{wi}$. The first correction to the fluid velocity fields are $O(\epsilon^{1/2})$ smaller than the leading contribution and the velocities are expanded in an asymptotic series as follows:

$$\tilde{v}_{oi} = \tilde{v}_{oi}^{(o)} + \epsilon^{1/2}\tilde{v}_{oi}^{(1)} + \cdots, \quad c = c^{(o)} + \epsilon^{1/2}c^{(1)} + \cdots . \tag{4.2}$$

The leading-order governing equation for the 'outer' solution is

$$(\mathrm{d}_r^2 + r^{-1}\mathrm{d}_r - r^{-2} - k^2)\tilde{v}_{or}^{(o)} - \frac{(U'' - r^{-1}U')}{(U - c^{(o)}/\Gamma)}\tilde{v}_{or}^{(o)} = 0, \tag{4.3}$$

where the base flow velocity profile U is obtained numerically. A fourth-order Runge–Kutta integrator was used to solve (4.3), using the value of the solution near $r \to 0$ as the initial condition. This initial condition was determined using a series expansion in r subject to the condition that $\tilde{v}_{or} = 0$ at $r = 0$. During the numerical integration, $c^{(o)}/\Gamma$ is fixed, and the solution for the radial velocity in the fluid is

$$\tilde{v}_{or} = A_1\phi^{(o)}, \tag{4.4}$$

where the constant A_1 has to be determined using the boundary conditions at the interface. Note that the solution of the differential equation (4.3) contains only one unknown constant, because the other has been fixed by the zero radial velocity condition along the axis. It is convenient to fix $c^{(o)}/\Gamma$ in the analysis and then treat Γ as the eigenvalue to be obtained from the problem. This is because the equation (4.3) is integrated only once in this procedure, and Γ is then calculated from the characteristic matrix (discussed below) obtained using the boundary conditions. The solutions for the axial velocity $\tilde{v}_{ox}$ and pressure $\tilde{p}^{(o)}$ are obtained from $\tilde{v}_{or}$ using the continuity and x-momentum equations respectively.

There is a wall layer of thickness $O(\epsilon^{1/2})$ at the interface and the governing equations in the wall layer can be obtained by rescaling the r-coordinate as $(1 - r) = \epsilon^{1/2}y$ in the governing equations. It turns out that the leading-order velocity and pressure in the wall layer are sufficient for the present analysis. The scaled equations in the wall layer of the present analysis are identical to those obtained in Kumaran (1995*b*) (see equations (2.27) to (2.29) of that paper), and we do not repeat them here. The wall layer governing equations can be solved analytically, and the solutions are given in Kumaran (1995*b*) (see equations (2.30) to (2.32) of that paper). The leading-order solutions of the displacement field in the gel are modified Bessel functions of the first and second kind (see Kumaran 1995*b*), and there are four constants in the wall eigenfunction to be determined from the boundary conditions at $r = H$ and the interface conditions at $r = 1$. The leading-order velocity and stress boundary conditions at the interface ($r = 1$) are

$$\tilde{v}_{or}^{(o)} = -\mathrm{i}kc^{(o)}\tilde{u}_r^{(o)}, \ \tilde{v}_{ox}^{(o)} + \tilde{v}_{wx} + U_w'\Gamma\tilde{u}_r^{(o)} = -\mathrm{i}kc^{(o)}\tilde{u}_x^{(o)}, \tag{4.5}$$

$$\tilde{\tau}_{orr}^{(0)} = \tilde{\sigma}_{rr}^{(0)}, \ \tilde{\sigma}_{xr}^{(0)} = 0. \tag{4.6}$$

The velocity and the pressure fields in the fluid, the velocity in the wall layer, and the displacement and pressure fields in the wall medium are substituted in the boundary conditions at $r = 1$ (4.5), (4.6) and in the zero displacement conditions at $r = H$. The eigenfunction for the wall layer velocity enters only in the tangential velocity boundary

condition in the leading approximation, and hence the other five boundary conditions are used to assemble the leading-order characteristic matrix $\boldsymbol{M}$ (of order 5×5). The eigenvalue Γ is determined by solving the characteristic equation $\mathrm{Det}(\boldsymbol{M}) = 0$, and the amplitude of the wall layer velocity is determined from the tangential velocity boundary condition. The characteristic equation admits multiple solutions for Γ for a given value of $c^{(o)}/\Gamma$ and thus $c^{(o)}$ can be found. It turns out that the characteristic equation admits only real values of $c^{(o)}$ as solutions thus indicating that the flow is neutrally stable in the leading approximation. Thus it is necessary to calculate the $O(\epsilon^{1/2})$ correction to the leading-order wave speed $c^{(o)}$ in order to determine the stability of the system.

The $O(\epsilon^{1/2})$ governing equations for the outer variables can be recast into a single second-order, inhomogeneous, ordinary differential equation:

$$(\mathrm{d}_r^2 + r^{-1}\mathrm{d}_r - r^{-2} - k^2)\tilde{v}_{or}^{(1)} - \frac{\Gamma(U'' - r^{-1}U')}{(\Gamma U - c^{(o)})}\tilde{v}_{or}^{(1)} = c^{(1)}\frac{\Gamma(U'' - r^{-1}U')}{(\Gamma U - c^{(o)})^2}\tilde{v}_{or}^{(o)}. \tag{4.7}$$

This equation is qualitatively different from the first correction equation of Kumaran (1995*b*) due to the presence of the inhomogeneous term in the right-hand side of the equation. For the parabolic profile (Kumaran 1995*b*), the term $(U'' - r^{-1}U')$ is identically zero and the first-correction equation is identical to the leading-order equation (4.3). For non-parabolic profiles, however, the equation (4.7) has to be solved numerically. Since $\tilde{v}_{or}^{(1)}$ is a linear function of $c^{(1)}$, the fluid velocity field in the outer layer correct to $O(\epsilon^{(1/2)})$ is

$$\tilde{v}_{or} = A_1(\phi^{(o)} + \epsilon^{1/2}c^{(1)}\phi^{(1)}), \tag{4.8}$$

where $\phi^{(o)}$ is the eigenfunction obtained from the leading-order equation (4.3) and $\phi^{(1)}$ is obtained by the numerical solution of (4.7). The $O(\epsilon^{(1/2)})$ corrections to the gel displacement field can be obtained analytically (see Kumaran 1995*b*). Using these eigenfunctions for the fluid and the gel, the characteristic matrix which includes the $O(\epsilon^{1/2})$ correction to the velocity and displacement field $\boldsymbol{M}$ is calculated, and the eigenvalues can be computed using $\mathrm{Det}(\boldsymbol{M}) = 0$. The results show that the real and imaginary parts of $c^{(1)}$ are equal in magnitude. It was also observed that the real and imaginary parts of $c^{(1)}$ are negative for all the mean velocity profiles and parameter values of Γ considered in the analysis, thus indicating that the flow is stable due to the presence of the wall layer. We found the regular modes to be always stable in the parameter space explored which typically ranged from $k = 1$ to 10 and $\Gamma = 1$ to 10. However, it was not possible to derive a stronger stability criterion, such as the energy balance analysis of Kumaran (1995*b*), for the present mean velocity profiles.

4.2. *Analysis of singular inviscid modes*

The wave speeds are in the range $0 < c_r/\Gamma < \max(U)$ for this class of modes and the critical point, at which $U = c_r/\Gamma$, is a regular singular point of the differential equation. It is well known (Drazin & Reid 1981, Chap. 4) that viscous effects are important in a 'critical layer' of thickness $O(Re^{-1/3})$ near a critical point. Two linearly independent solutions to the differential equation can be obtained using a Frobenius expansion in the variable $(r - r_c)$ near the singular point r_c:

$$\phi_1(r) = (r - r_c)P_1(r), \tag{4.9}$$

$$\phi_2(r) = P_2(r) + \left(\frac{U_c'' - r_c^{-1}U_c'}{U_c'}\right)\phi_1(r)\log(r - r_c), \tag{4.10}$$

where $P_1(r)$ and $P_2(r)$ are series expansions in $(r - r_c)$. $P_1(r)$ is analytic at $r = r_c$, the second linearly independent solution $\phi_2(r)$ has a logarithmic branch point at $r = r_c$ and $P_2(r)$ is analytic at $r = r_c$. The coefficients of the terms in $P_1(r)$ and $P_2(r)$ can be readily found using symbolic computation. The term $\log(r - r_c)$ is regular when $(r - r_c) > 0$, but could have multiple values $\log(r - r_c) = \log|r - r_c| \pm i\pi$ when $(r - r_c) < 0$, and it is necessary to specify the correct branch of the multi-valued solution given by $\phi_2(r)$ (Drazin & Reid 1981, Chap. 4). The inviscid theory does not prescribe the proper branch of the logarithm, and it is necessary to investigate the region near $r = r_c$ in more detail. The fourth-order OS-like equation is rescaled near $r = r_c$ by introducing the 'inner variable' $\psi \sim (r - r_c)/Re^{-1/3}$ in the critical layer, and the viscous terms enter into the leading-order equations near $r = r_c$. The resulting fourth-order differential equation is solved, and the inviscid limit of these solutions is taken to identify the proper branch of the logarithm in the inviscid eigenfunction $\phi_2(r)$. The result shows that $\log(r - r_c) = \log|r - r_c| + i\pi$, for the axisymmetric case which is of interest here. Thus the effects of viscous stresses near r_c are incorporated in the inviscid calculation by choosing the correct branch for the logarithm in the singular eigenfunction ϕ_2. A similar procedure is used in the 'triple deck' analysis of Carpenter & Gajjar (1990) for the stability of boundary layer flow past a compliant surface when the critical layer is well separated from the wall layer.

The solution for the velocity in the tube is obtained by numerical integration using the series solutions in the critical layer as the initial conditions. The ranges of r for the numerical integration are $r = r_c + \epsilon$ to $r = 1$ and from $r = r_c - \epsilon$ to $r = 0$, where ϵ is a small quantity $\sim 10^{-4}$. Near $r \to 0$, the differential equation has two eigenfunctions. One of these decays ($\sim r$) and the other grows ($\sim 1/r$). During the numerical integration from $r = r_c - \epsilon$ to $r = 0$, the numerical eigenfunctions acquire the 'growing eigenfunction' $(1/r)$ behaviour as $r \to 0$ and care has to be taken to separate out the $1/r$ behaviour. The eigenfunctions for the wall displacement field obtained analytically for regular modes are used for this calculation. Using the boundary conditions at $r = 0$, $r = 1$ and $r = H$, a 6×6 characteristic matrix is assembled whose determinant is set to zero in order to find the eigenvalues. It was found convenient to fix the value of c_r/Γ and treat Γ as the unknown eigenvalue. After the singular neutral modes are identified, it is necessary to determine whether a small variation in the flow parameters renders these modes unstable. For modes that are not neutral, $c_i \neq 0$, there is no singular point for the governing equation (4.3) and the stability of these modes is determined using a numerical procedure that is identical to the calculation of regular neutral modes. In this procedure, the parameter Γ is varied by a small amount from its value for the neutral modes and the imaginary part of the wave speed c_i is determined. This calculation shows that the neutral mode does become unstable for a small increase in the parameter Γ, and the flow is unstable in the inviscid limit. This result is observed for both developing flows and flows in converging tubes, and this verifies the prediction in Kumaran (1996) that these flows could be unstable in the inviscid limit. It is of interest to determine whether this instability is captured by an analysis of the complete stability equations and the values of the Reynolds number up to which this instability persists. This is accomplished using a numerical solution of the complete equations governing the stability.

5. Numerical solution of the complete stability equations

Equations (3.11) and (3.12) are two fourth-order ordinary differential equations for the fluid velocity field and the wall displacement field respectively. There are two

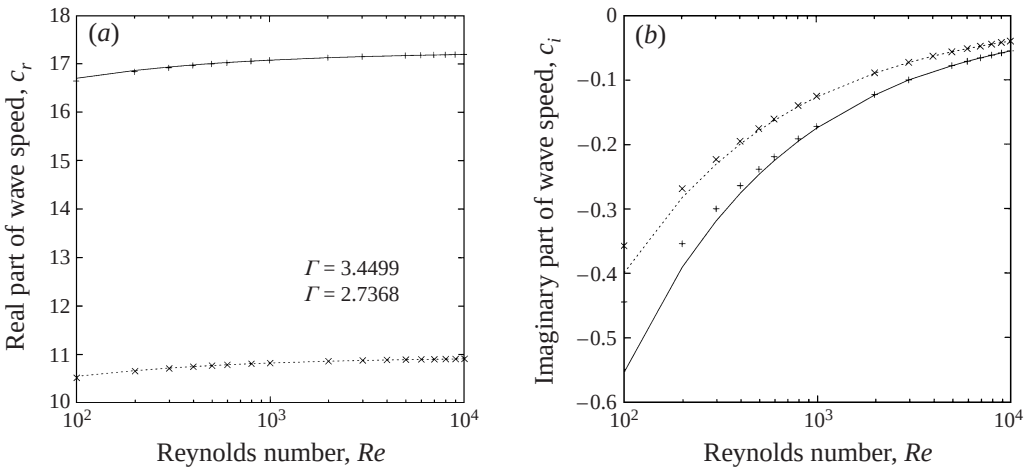

FIGURE 1. Comparison of asymptotic (+, ×) with numerical (—, ⋯) results: (*a*) real part and (*b*) imaginary part of wave speed vs. Re; $X = 0.001$, $k = 1$, $H = 2$.

solutions for the fluid velocity field consistent with the symmetry conditions at the centre of the tube, and two solutions for the gel displacement field consistent with the zero displacement condition at $r = H$. The numerical method used for determining these eigenfunctions is a fourth-order Runge–Kutta integrator with adaptive step size control along with a Gram–Schmidt orthonormalization procedure. The eigenfunctions for the fluid velocity field and gel displacement field are substituted into the four boundary conditions at the interface between fluid and the gel and a 4×4 characteristic matrix is obtained. The determinant of this matrix is set equal to zero to obtain the wave speed c. A Newton–Raphson iteration technique was used to obtain the solution using the known solutions in the high Reynolds number limit as the initial guess.

Two tests were carried out to verify the accuracy of the numerical method. The first compares the results from this numerical method with the asymptotic results discussed in § 4.1 for regular inviscid modes. In § 4.1, the wave speed c was calculated using an asymptotic expansion for regular modes, and these results are correct to $O(Re^{-1/2})$. Thus the asymptotic solution to the wave speed c is in error by a factor of $O(Re^{-1})$. Figure 1 shows the comparison between the asymptotic results c_a and numerical results c_n for the real and imaginary parts of the wave speed. There is excellent agreement between the asymptotic and numerical results for $Re > 1000$. The ratio of the magnitude of the error in the asymptotic growth rate and the magnitude of the numerical growth rate was computed and it decreases proportional to Re^{-1} for $Re \gg 1$, as it should, since the asymptotic analysis is correct only to $O(Re^{-1/2})$. Thus, our numerical method is consistent with the asymptotic results obtained in § 4.1. The results of our numerical scheme were also compared with the numerical results of the linear stability of developing flow in a rigid tube. It is appropriate to compare our numerical scheme with that of Garg (1981), since the base flow used there was also obtained using the method of Hornbeck (1963). Though the analysis of Garg (1981) was a spatial stability analysis, it is possible to compare the present results with it because both spatial and temporal stability analyses yield the same result for the wave speed for neutral modes. The rigid tube results of Garg (1981) can be recovered from the numerical procedure used in this study by considering

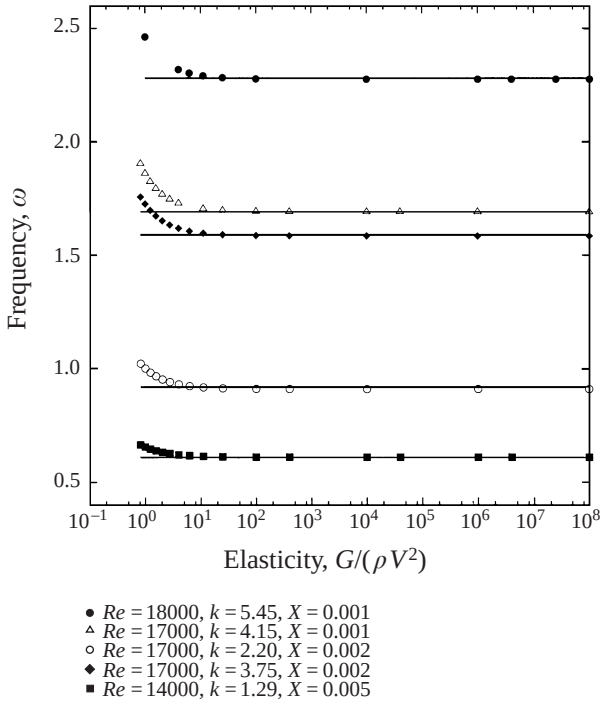

FIGURE 2. Comparison of rigid tube results of Garg (1981) for different values of X (lines) with flexible tube results (symbols).

limit of large elasticity, i.e. $G/(\rho V^2) \gg 1$ at a fixed value of H. Figures 3 and 4 in Garg (1981) were electronically scanned and the neutral values were extracted from the digitized image. In figure 2, the flexible tube solution is shown as a function of the parameter $G/(\rho V^2)$. Our numerical procedure captures the frequency of the rigid tube results very well and the frequency converges to the rigid tube value even when $G/(\rho V^2) \sim 10$. The rigid tube results were also recovered by fixing $G/(\rho V^2)$ and taking the limit as $(H-1) \to 0$. Therefore, the numerical method is consistent with the asymptotic results for a flexible tube obtained in this paper, as well as with the previous numerical stability analyses for a rigid tube.

6. Results

6.1. *Developing flow velocity profile*

First, we consider the results obtained for the stability of developing flow velocity profiles. It is convenient to define a 'transition Reynolds number' (Re_t) which refers to the transition from stable to unstable modes for a given wavenumber k. The Re_t at which the developing flow profile at an axial position becomes unstable depends on the following parameters: the wavenumber k, the dimensionless base flow velocity Γ, the ratio of wall thickness to fluid thickness H, and the ratio of gel to fluid viscosities η_r. The values of the wave speed obtained from the asymptotic analysis of the singular inviscid modes were used as initial guesses for the numerical analysis, and the initial Reynolds number was set to 10^5. A numerical continuation procedure was then used to obtain the neutral curve at lower values of the Reynolds number. The results are plotted in terms of Re vs. Σ, where $\Sigma = (\rho G R^2/\eta^2) = (Re/\Gamma)^2$ is

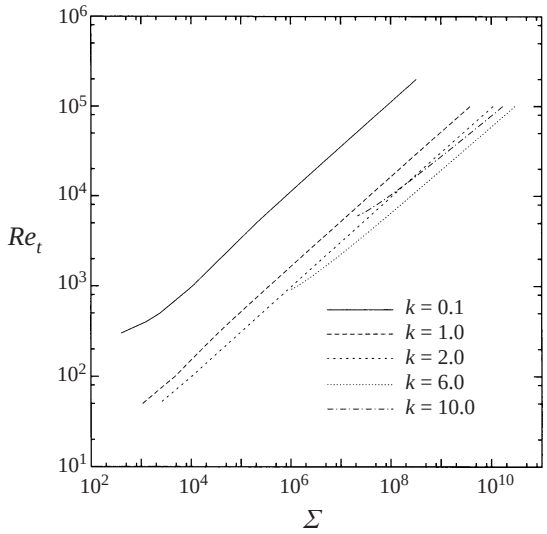

FIGURE 3. Transition Reynolds number Re_t vs. Σ for different k; X = 0.050, $H = 2$.

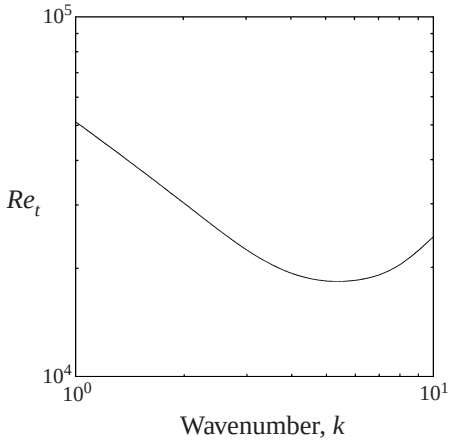

FIGURE 4. Transition Reynolds number Re_t vs. wavenumber k for a developing flow velocity profile at $X = 0.05$, $\Sigma = 10^9$, $H = 2$.

a parameter that depends only on the material properties of the fluid and the wall, and it is independent of the flow parameters. The case $\eta_r = 0$, where the wall is purely elastic, is discussed first. Figure 3 shows the Reynolds number for neutrally stable modes as a function of Σ for $X = 0.050$ and different wavenumbers k, where $X = x^*/(RRe)$ is the non-dimensional axial distance from the entrance of the tube. The area below each of the curves represents the stable region and the area above the curve represents the unstable region. For a given Σ, the Re_t has a minimum at finite k, indicating that the most unstable modes have finite wavelength. This plot can be used to determine the critical Reynolds number Re_c, which is the Reynolds number below which fluctuations are stable for all k. In figure 4 the transition Reynolds number is plotted against the wavenumber for a given Σ, and the minimum of this curve is Re_c with k_c being the corresponding critical wavenumber. Our calculations indicate that k_c is an $O(1)$ quantity, thus supporting the validity of the parallel flow approximation.

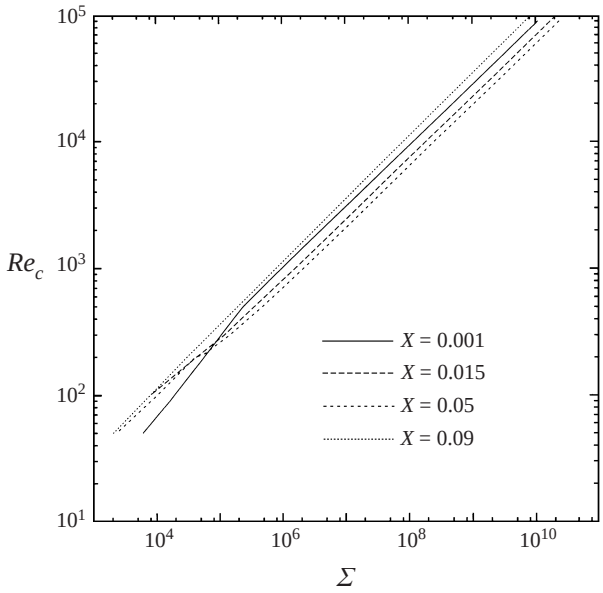

FIGURE 5. Critical Reynolds number Re_c vs. Σ for different axial positions for $H = 2$.

The conventional Re vs. k graphs for the present neutral modes look very similar for all the cases considered, with the minimum Re occurring at some $k \sim O(1)$. This is in contrast to the results of LaRose & Grotberg (1997) where there could be two minima in the (Re, k)-plane. Consequently, in the following discussion we present only the results of Re_c vs. Σ for velocity profiles at different axial positions.

The behaviour of the Reynolds number for the neutral modes in the limiting cases of $k \ll 1$ and $k \gg 1$ for a given Σ can be obtained by a simple asymptotic analysis of the inviscid governing equations. The analysis in the Appendix shows that the scaling of the Reynolds number with k in the limiting cases $k \ll 1$ and $k \gg 1$ is respectively $Re \sim k^{-1}$ and $Re \sim k$. This scaling is completely different from the conventional 'lower' and 'upper' branch scalings for developing flow stability in a rigid tube. Therefore, the present modes are not a perturbation of the already known branches for the stability of developing flow in a rigid tube. Figure 5 shows the variation of Re_c with Σ for different axial stations. In figure 6 we show the variation of the critical Reynolds number with the axial distance from the entry for a given value of Σ. It is found that Re_c initially decreases with X, and then increases, indicating that the developing flow at an intermediate axial station is the most unstable profile. It is of interest to compare the present critical Re curve with the critical Re obtained for the stability of developing flow through a rigid tube. The computations of Garg (1981) show that the critical Reynolds number is around 12 000 for the most unstable developing velocity profile. It can be seen from figure 5 that the critical Re in a flexible tube can be much lower than that in a rigid tube and the flexible tube curve does not approach the rigid tube value in any asymptotic limit, indicating that the present instability is qualitatively different from that of the rigid tube instability. This is also reflected in the fact that there is no transition from unstable to stable modes in the (Re, k)-plane as the Reynolds number is increased in a flexible tube, in contrast to the developing flow in a rigid tube where there is a second transition from unstable

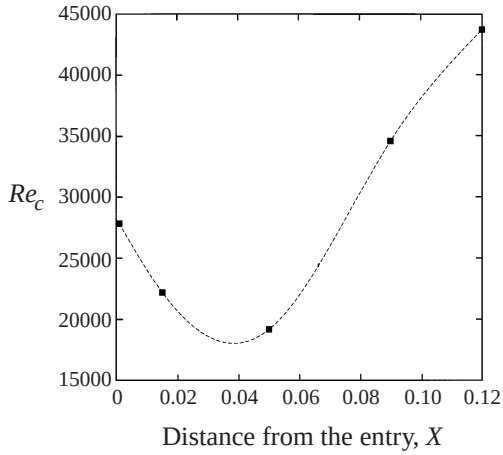

FIGURE 6. Critical Reynolds number Re_c vs. distance from the entry, X, for $\Sigma = 10^9$, $H = 2$.

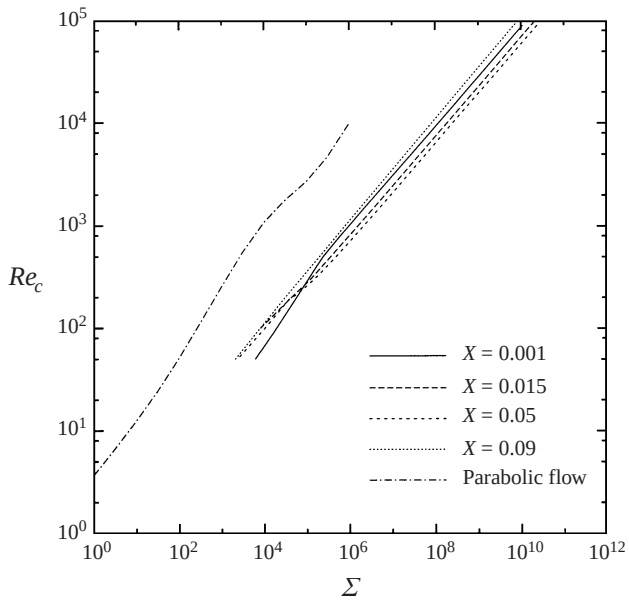

FIGURE 7. Critical Reynolds number Re_c vs. Σ: Comparison with the results of Kumaran (1998*b*) for parabolic flow in a flexible tube for $H = 2$.

to stable modes as the Reynolds number is increased in the (Re, k)-plane, and the unstable region is restricted to a finite band of Re.

Figure 7 shows the critical Re vs. Σ results for the developing flow profile, along with the results obtained by Kumaran (1998*b*) for the parabolic profile. In that analysis, the unstable modes were a continuation of the low-Re viscous unstable modes (Type A in our classification) to the intermediate Reynolds number regime. This figure shows that the developing flow always has a much lower Re_c than the parabolic flow for a given Σ. At high Re there is a significant region where the flow is developing, and the present instability can play an important role in the stability of fluid flow through flexible tubes. A comparison cannot be made at a Reynolds

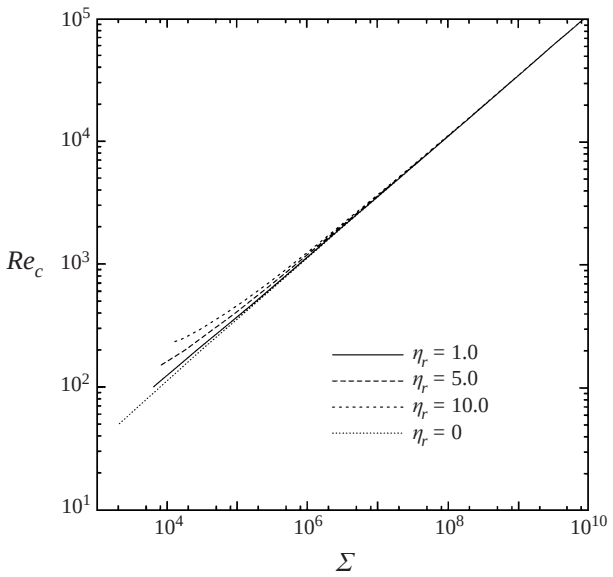

FIGURE 8. Effect of ratio of viscosity of wall medium to fluid, η_r, on the critical Reynolds number for a developing flow velocity profile at $X = 0.09$, $H = 2$.

number of $O(1)$ or lower, because the entrance length for the development of the velocity profile is of the same magnitude as the tube radius, and the parallel flow approximation would not be valid. However, when the flow Re is $O(10^2)$ or higher, the error incurred due to the parallel flow approximation is small (as discussed in § 7), and our analysis reveals that the inviscid instability of a developing flow velocity profile is more unstable than the viscous instability of a fully developed flow. In the analysis of Kumaran (1998*b*), the critical Re for parabolic flow was found to scale as $Re_c \sim \Sigma^a$, where the exponent a was found to vary between 0.7 to 0.75. In the present case, the scaling relation turns out to be $Re_c \sim \Sigma^{1/2}$.

It is useful at this point to compare the instability observed in this paper and the instability of developing flow in a rigid tube analysed in Smith & Bodonyi (1980) and Garg (1981). The Reynolds number Re_c for singular inviscid modes in a flexible tube scales as $\Sigma^{1/2}$ where $\Sigma \equiv (\rho R^2/\eta^2)G$ is a non-dimensional parameter proportional to the shear modulus of the wall medium. The critical Reynolds number increases as the square root of the wall elasticity for the inviscid instability of developing flow in a flexible tube. However, $G \to \infty$ is the rigid tube limit, and the earlier linear stability analyses of developing flow in a rigid tube indicate that the critical Reynolds number is around 12 000. This clearly demonstrates that the singular inviscid modes obtained in this paper will not reduce, in any asymptotic limit, to the results of the stability of developing flow in a rigid tube. Therefore, the instability analysed in this paper is qualitatively different from that of developing flow in a rigid tube. Figure 8 shows Re_c vs. Σ for various values of the ratio of gel to fluid viscosities η_r. An increase in η_r increases the Re_c for a given Σ, indicating that the viscosity of the wall has a stabilizing effect on the present instability. This is in contrast with the results of Kumaran (1998*b*), where η_r was found to have a complex dependence on the stability characteristics. In our analysis, neutral stability curves have been computed for Re as low as 100 using the parallel flow approximation. At such low Re, the previously neglected 'non-parallel' terms could influence the stability of the flow. The variation in

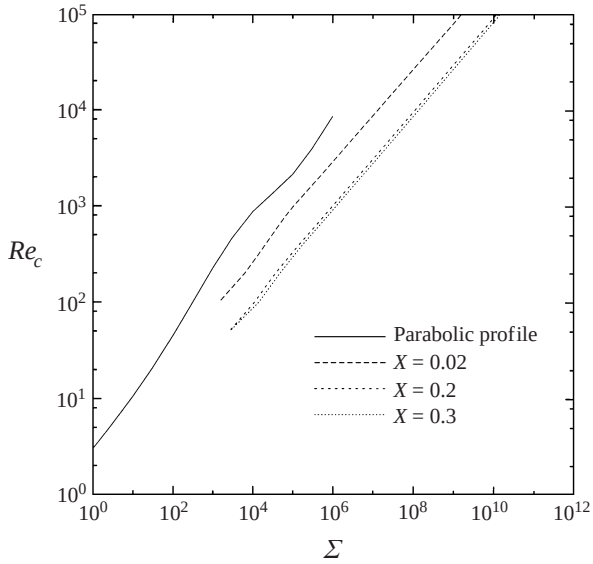

FIGURE 9. Re_c vs. Σ for converging tube velocity profiles at different axial distances. $H = 2$, $\eta_r = 0$.

the neutral stability curves due to the largest of the non-parallel terms is determined in § 7.

6.2. *Slightly converging tube*

The stability of velocity profiles that occur in a tube which is slightly tapering along the axial direction is considered here. This convergence could occur in flexible tubes due to applied pressure gradients, and in the experiments of Krindel & Silberberg (1979), the authors observed a convergence and estimated that the slope was around 1×10^{-3}. As mentioned in § 3, the convergence of the tube significantly influences the base velocity profile when $\alpha Re \sim 1$. In the present calculations, the velocity profile at the inlet is considered to be parabolic, and it turns progressively non-parabolic further downstream in the tube. In figure 9 the Re_c vs. Σ curves at various axial distances are shown. The inviscid instability mechanism is operative even if the velocity profile is only slightly different from the inlet parabolic flow. The critical Re is always less than that for a parabolic flow for a given Σ. As the flow becomes progressively non-parabolic, the critical Re decreases for a given Σ.

7. Error due to the parallel flow assumption

In the parallel flow stability analysis, the terms that contained the gradient of the mean flow axial velocity and the mean radial velocity were neglected, because it was assumed that they are $O(Re^{-1})$ smaller than leading-order terms in the limit $Re \gg 1$. It might then be expected that there is a correction of $O(Re^{-1})$ in the governing equations due to the inclusion of the non-parallel terms, and this would result in a set of partial differential equations for the velocity perturbations. However, some recent work by Govindarajan & Narasimha (1997) suggests that the largest correction to the governing equations is $O(Re^{-1/3})$ smaller than the leading-order terms, and the parallel flow approximation can still be used to evaluate this correction, as discussed below.

Consider the following linearized partial differential equations governing the x- and r-components of the velocity perturbations. Here the quantities with an overbar are mean flow velocities and those without are velocity perturbations:

$$\partial_t v_x + v_x \partial_x \bar{v}_x + \bar{v}_x \partial_x v_x + \bar{v}_r \partial_r v_x + v_r \partial_r \bar{v}_x = -\partial_x p + \Gamma Re^{-1}[\partial_r^2 + r^{-1}\partial_r + \partial_x^2]v_x, \quad (7.1)$$

$$\partial_t v_r + \bar{v}_r \partial_r v_r + v_r \partial_r \bar{v}_r + \bar{v}_x \partial_x v_r + v_x \partial_x \bar{v}_r = -\partial_r p + \Gamma Re^{-1}[\partial_r^2 + r^{-1}\partial_r - r^{-2} + \partial_x^2]v_r. \quad (7.2)$$

The mean flow quantities for the non-parabolic flows of interest in this study are scaled as follows: $\bar{v}_x = \Gamma U$, $\bar{v}_r = \Gamma Re^{-1} V$, $\partial_x \bar{v}_x = \Gamma Re^{-1} \partial_x U$, $\partial_x \bar{v}_r = \Gamma Re^{-2} \partial_r V$. The 'normal modes' for the disturbance velocities are (see Gaster 1972; Govindarajan & Narasimha 1997)

$$v_i = \tilde{v}_i(r, x) \exp\left[\mathrm{i} \int k(x)\, \mathrm{d}x - \mathrm{i}\omega t\right], \quad (7.3)$$

where $\tilde{v}_i(x, r)$ is in general a function of r and x, ω is the frequency of perturbations and the wavenumber $k(x)$ is also a function of x in general. In the above equation, $\omega \equiv \mathrm{i}kc$, is the frequency of perturbations. On substituting this form for the disturbances in the linearized partial differential equations, and retaining all quantities that are of $O(Re^{-1})$, a single fourth-order *partial* differential equation can be obtained in terms of $\tilde{v}_x$ and $\tilde{v}_r$. This equation contains terms representing the derivatives of the eigenfunction in the x-direction and the derivative of the wavenumber in the x-direction. Since the axial derivative of the mean velocity along the x-direction is $O(Re^{-1})$ smaller than its radial derivative, the axial derivatives of the disturbance velocities will at most be of $O(Re^{-1})$ smaller than the leading-order contributions. However, as shown below, there are larger corrections due to the axial variation of the mean velocity in the critical layer.

Since the thickness of the critical layer is $O(Re^{-1/3})$ smaller than the radius of the tube, it is appropriate to use a new coordinate $\eta = (r - r_c)/Re^{-1/3}$. The eigenfunctions are expanded in an asymptotic series as follows:

$$\tilde{v}_r = \chi(\eta) = \chi_o(\eta) + Re^{-1/3}\chi_1(\eta) + \cdots . \quad (7.4)$$

The mean flow velocity is expanded near the critical layer as

$$U = U_c + U_c'(r - r_c) + U_c''(r - r_c)^2/2 + \cdots . \quad (7.5)$$

The leading-order and $O(Re^{-1/3})$ correction to the governing equations near the critical layer can then be obtained:

$$\mathrm{d}_\eta^4 \chi_0 - \mathrm{i}kU_c' \eta\, \mathrm{d}_\eta^2 \chi_0 = 0, \quad (7.6)$$

$$\frac{U_c''}{2}\eta^2\, \mathrm{d}_\eta^2 \chi_0 + U_c' \eta\, \mathrm{d}_\eta^2 \chi_1 - (U_c'' - r_c^{-1} U_c')\chi_0 + \left[\frac{\mathrm{i}V\, \mathrm{d}_\eta^3 \chi_0}{k}\right] = \frac{1}{\mathrm{i}k}(\mathrm{d}_\eta^4 \chi_1 + 2r_c^{-1}\mathrm{d}_\eta^3 \chi_0), \quad (7.7)$$

where $\mathrm{d}_\eta = \mathrm{d}/\mathrm{d}_\eta$. The leading-order equation (7.6) is identical to that obtained in the parallel flow approximation. However the first correction equation contains an additional term that is due to the radial velocity in the critical layer (the term inside the square brackets in (7.7)). Thus, the largest non-parallel term is $O(Re^{-1/3})$ smaller than the leading-order terms in the equations for a parallel flow. This $O(Re^{-1/3})$ term is incorporated, and the next correction in the critical layer is of $O(Re^{-2/3})$ and is neglected here. A similar analysis can easily be carried out in the wall layer to

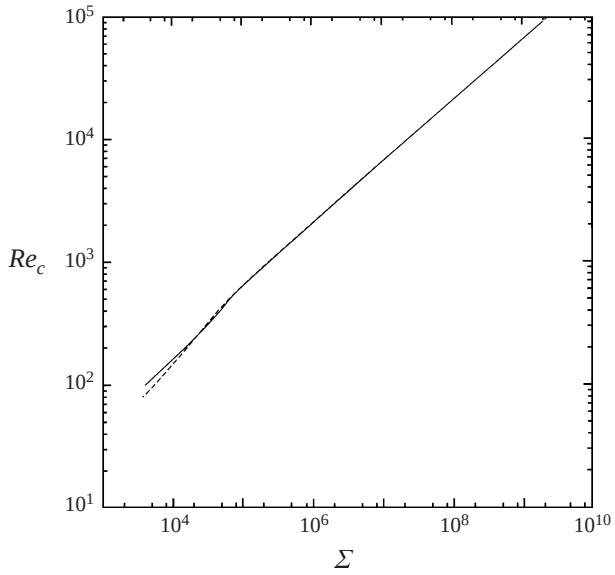

FIGURE 10. Re_c vs. Σ for developing flow velocity profile at $X = 0.015$, $H = 2$: parallel (———) and non-parallel (- - - -) results.

estimate the error due to the parallel approximation. This analysis reveals that the $O(1)$ and $O(Re^{-1/2})$ equations in the wall layer do not contain any terms due to axial gradients in the mean velocity profile or the radial component of the mean velocity, and hence the error due to the parallel flow approximation is $O(Re^{-1})$ smaller than the leading-order terms in the wall layer.

The above scaling arguments show that the largest correction to the equations due to the neglect of the axial gradient of the mean flow and the radial component of the mean flow is $O(Re^{-1/3})$ smaller than the leading-order terms, and this leading-order correction is due to the term $\bar{v}_r \partial_r v_x$ in the linearized partial differential equation (7.1). If we incorporate this largest correction, the error incurred is at most of $O(Re^{-2/3})$, since we have neglected certain terms which are of $O(Re^{-2/3})$ in the critical layer. On including such a term in the OS-type equation, one obtains after defining $\mathscr{L} = (\partial_r^2 + r^{-1}\partial_r - r^{-2} - k^2)$

$$\left(U - \frac{\omega}{k\Gamma}\right)\mathscr{L}\tilde{v}_r - (U'' - r^{-1}U')\tilde{v}_r = \frac{1}{\mathrm{i}kRe}[\mathscr{L}^2\tilde{v}_r + V\partial_r(\partial_r^2 + r^{-1}\partial_r - r^{-2})\tilde{v}_r]. \quad (7.8)$$

This fourth-order equation is an ordinary differential equation, and it contains all terms that are $O(Re^{-1/3})$ and $O(Re^{-1/2})$ smaller than the leading-order terms in the critical and wall layers. This equation also contains some additional terms which are of higher order than $O(Re^{-1/2})$, but since the problem is to be solved numerically this is not a major issue. This equation incorporates the spatial development of the flow due to the dependence of U on x, the dependence of k on x and the dependence of the eigenfunction on x.

For a non-parallel flow, spatial neutral stability is defined as $\partial_x\phi/\phi = 0$ where ϕ is the perturbation to the variable under consideration. The eigenfunction has the form

$\phi = \tilde{\phi}(r, x) \exp\left[\mathrm{i} \int k(x)\, \mathrm{d}x - \mathrm{i}\omega t\right]$, and the criterion $\partial_x \phi / \phi = 0$ becomes

$$\mathrm{Re}\left(\mathrm{i}k + \frac{\partial_x \tilde{\phi}}{\tilde{\phi}}\right) = 0, \tag{7.9}$$

where Re denotes the real part of a complex number. The neutral stability curve then depends on the variable under consideration and the radial coordinate (r). In this analysis of the non-parallel flow, the gradients of the eigenfunctions ($\partial_x \tilde{\phi}$) are neglected since these terms are $O(Re^{-1})$ smaller than the leading-order terms. Therefore, the definition of the neutral stability reduces to $k_i = 0$, which is the same as the definition for the parallel flow approximation. This definition for spatial neutral stability coincides with the temporal neutral stability, for which $\omega_i = 0$. Figure 10 shows the neutral curve Re_c vs. Σ obtained using the above definition of stability $c_i = 0$ along with the neutral curve obtained from the parallel flow approximation, for $X = 0.015$. It is observed from these plots that the non-parallel effects are indeed marginal, and they become significant only near $Re \sim 10^2$.

8. Conclusions

The stability of non-parabolic velocity profiles in a flexible tube was analysed in the limit of high Reynolds numbers using asymptotic analyses, and the results were extended to the moderate Reynolds number regime using a numerical approach. Two specific flows were considered: (i) the developing flow velocity profiles that occur prior to the formation of a parabolic velocity profile, and (ii) the velocity profiles that occur in a slightly converging tube. Both these flows were treated as locally parallel, and the classical temporal stability theory was used to determine their stability; an asymptotic analysis showed that the non-parallel effects do not alter the neutral stability curves significantly. In the limit of high Reynolds numbers, two classes of modes are possible: the regular inviscid modes (Type D), which are akin to the inviscid modes observed in Kumaran (1995*b*) for parabolic flow in a flexible tube, and singular inviscid modes (Type E) which do not appear for parabolic flows. An asymptotic analysis in the small parameter $Re^{-1/2}$ indicated that the regular inviscid modes are always stable. This is in contrast with the studies of Davies & Carpenter (1997) and Carpenter & Garrad (1986) which found instability for the regular inviscid modes for flow past spring-backed walls.

The singular inviscid modes cannot be studied using the above asymptotic expansion, and special care has to be taken to determine the eigenfunctions in the inviscid limit. The singular inviscid modes were found to give rise to an instability in the inviscid limit, thus verifying such a prediction in Kumaran (1996). Interestingly, both the non-parabolic velocity profiles are stable in a rigid tube in the inviscid limit. The main reason for the instability of non-parabolic profiles is the presence of the critical layer in the fluid due to the singularity in the inviscid stability equations, which is absent for parabolic flows. This critical layer gives rise to a convective transport of energy from mean flow to fluctuations in certain cases, thus rendering the flow unstable. For a detailed discussion on energy balance arguments, the reader is referred to Kumaran (1995*b*). For developing flow in a rigid tube, the neutral stability curve has characteristic 'upper' and 'lower' branches, and the flow is unstable only over a finite range of Reynolds numbers at a fixed wavenumber. The neutral stability curve in the present case is qualitatively different from this rigid tube behaviour, and the transition Reynolds number scales proportional to k^{-1} at small wavenumber, has a minimum at

finite wavenumber and increases proportional to k for large wavenumber. The critical Reynolds number scales proportional to $\Sigma^{1/2}$ in the limit of large elasticity $\Sigma \gg 1$, in contrast to the finite value assumed by the critical Reynolds number in the rigid tube case.

A numerical method was devised to continue the results from the high-Re to the intermediate-Re regime. The numerical results reveal that the inviscid instability mechanism can exist even at very moderate Re like 100. Importantly, the critical Reynolds number for the case of non-parabolic velocity profiles is very low when compared with the parabolic profile results of Kumaran (1998*b*) for a given Σ, and hence the inviscid instability mechanism could be very powerful in rendering the flow in a flexible tube unstable. This is because at moderate to high Re, there is a significant region in the entrance of the tube where the velocity profile is not parabolic, and in these situations, the present instability mechanism could be very important. In the case of velocity profiles in a slightly converging tube, even slight deviations from the parabolic velocity profiles were found to be sufficient for the inviscid instability mechanism to be operative. More importantly, the critical Re for the converging flow profiles were found to be much less than the critical Re for the parabolic flow. The dominant effects of flow non-parallelism are incorporated to $O(Re^{-1/2})$ using an asymptotic analysis, and it was found that non-parallel terms do not have a significant effect on the neutral stability curves.

Appendix. Low- and high-wavenumber asymptotic analysis

The behaviour of the Reynolds number of the neutral modes in the limiting cases of $k \ll 1$ and $k \gg 1$ for a given Σ can be obtained by a simple asymptotic analysis of the inviscid governing equations for the singular inviscid modes. The following analysis shows that the shape of the neutral curve for the present instability is completely different from that observed for instabilities on rigid surfaces. Specifically, we show below that the scaling of the Reynolds number with k in the limiting cases $k \ll 1$ and $k \gg 1$ is respectively $Re \sim k^{-1}$ and $Re \sim k$. This scaling is completely different from the conventional 'lower' and 'upper' branch scalings for flow past rigid surfaces. We first turn to the low-wavenumber (or, long-wavelength) analysis of the inviscid governing equations.

Low-wavenumber analysis

The non-dimensional inviscid governing equations for the fluid are the following:

$$(\mathrm{d}_r + r^{-1})\tilde{v}_r + \mathrm{i}k\tilde{v}_x = 0, \tag{A 1}$$

$$\mathrm{i}k(\Gamma U - c)\tilde{v}_r = -\mathrm{d}_r\tilde{p}_f, \tag{A 2}$$

$$\mathrm{i}k(\Gamma U - c)\tilde{v}_x + \Gamma U'\tilde{v}_r = -\mathrm{i}k\tilde{p}_f. \tag{A 3}$$

At the interface ($r = 1$), the continuity of normal velocity is given by $\tilde{v}_r = -\mathrm{i}kc\tilde{u}_r$. In order for the wall deformations to affect the fluid flow, c should scale as k^{-1}. Thus, we expand

$$c = k^{-1}c^{(0)} + c^{(1)} + \cdots . \tag{A 4}$$

From the continuity equation, it can be seen that $\tilde{v}_x = O(k^{-1})\tilde{v}_r$, and we expand

$$\tilde{v}_x = k^{-1}\tilde{v}_x^{(0)} + \tilde{v}_x^{(1)} + \cdots, \tag{A 5}$$

$$\tilde{v}_r = \tilde{v}_r^{(0)} + k\tilde{v}_r^{(1)} + \cdots . \tag{A 6}$$

The continuity equation then reads

$$(\mathrm{d}_r + r^{-1})\tilde{v}_r^{(0)} + \mathrm{i}\tilde{v}_x^{(0)} = 0. \tag{A 7}$$

Consider now the x-momentum equation. On using the expansion for c, $\tilde{v}_x$ and $\tilde{v}_r$ the x-momentum equation becomes

$$\mathrm{i}(\Gamma U - k^{-1}c^{(0)})\tilde{v}_x^{(0)} + \Gamma U'\tilde{v}_r^{(0)} = -\mathrm{i}k\tilde{p}_f. \tag{A 8}$$

The first term in the left-hand side indicates that for singular modes to exist in the limit of low k, i.e. for $\Gamma U = c^{(0)}k^{-1}$ somewhere in the flow, Γ should to scale as k^{-1} in the low-k limit. Therefore, we expand

$$\Gamma = \Gamma^{(0)}k^{-1} + \Gamma^{(1)} + \cdots . \tag{A 9}$$

The scaling for $\tilde{p}_f$ should be of $O(k^{-2})$ in order for a balance to exist between the left- and right-hand sides of the x-momentum equation. So, $\tilde{p}_f$ is expanded as

$$\tilde{p}_f = k^{-2}\tilde{p}_f^{(0)} + \cdots . \tag{A 10}$$

The scaled x-momentum equation then becomes in the low-k limit

$$\mathrm{i}(\Gamma^{(0)}U - c^{(0)})\tilde{v}_x^{(0)} + \Gamma^{(0)}U'\tilde{v}_r^{(0)} = -\mathrm{i}k\tilde{p}_f^{(0)}. \tag{A 11}$$

The r-momentum equation simply gives $\mathrm{d}_r\tilde{p}_f^{(0)} = 0$ in the leading approximation. The governing equation for $\tilde{v}_r^{(0)}$ in the limit of low k can then be obtained by combining the scaled continuity, x-momentum and r-momentum equations:

$$(\Gamma^{(0)}U - c^{(0)})(\mathrm{d}_r^2 + r^{-1}\mathrm{d}_r - r^{-2})\tilde{v}_r^{(0)} - \Gamma^{(0)}(U'' - r^{-1}U')\tilde{v}_r^{(0)} = 0. \tag{A 12}$$

Thus, from the analysis of the x-momentum equation, we have obtained the scaling for Γ in the limit of low k and we find that $\Gamma \sim k^{-1}$ in this limit. The governing equations for the wall medium can be similarly scaled, but since we have obtained the scaling for Γ, we do not need them here. For the inviscid modes studied in this paper, the scaling for the Reynolds number is given by $Re = \Sigma^{1/2}\Gamma$. For a fixed Σ, this implies $Re \sim \Gamma$. Since $\Gamma \sim k^{-1}$ in the low-k limit, we obtain the scaling for Re in the $k \to 0$ limit as $Re \sim k^{-1}$. This is the scaling for the 'lower branch' (the $k \to 0$ branch) in the Re vs. k neutral curve for a fixed Σ. This $Re \sim k^{-1}$ behaviour is completely different from the conventional lower branch scalings for developing flow in a rigid tube, which is $Re \sim k^{-1/8}$. We now turn to the scaling of the Reynolds number in the limit $k \gg 1$.

High-wavenumber analysis

We note that $k \equiv k^*R$ (k^* is the dimensional wavenumber of perturbations and R is the radius of the tube), and in the high-wavenumber limit $k \gg 1$. This implies that we are considering waves of wavelengths much smaller than the tube radius. Consequently, in this limit, the curvature effects of the axisymmetric geometry do not appear in the leading-order governing equations (when scaled appropriately; see below), and the system appears identical to flow past a planar flexible surface. All the variation in the dynamical quantities takes place in a region very near the interface between the fluid and the wall. In this limit, the appropriate length scale is not R (the radius of the tube), but $1/k^*$ (the wavelength of perturbations). Therefore, we define a new independent variable $\eta = (1 - r^*/R)k$, i.e. $\eta = (1 - r)k$, where η is an $O(1)$ quantity and $k \gg 1$. This scaling ensures that we are very near the fluid–wall interface ($r^*/R = 1$).

The dimensional continuity and momentum equations for the Fourier components of the velocities are given by

$$\mathrm{d}_r^* \tilde{v}_r^* + r^{*-1}\tilde{v}_r^* + \mathrm{i}k^*\tilde{v}_x^* = 0, \tag{A 13}$$

$$\rho \mathrm{i}k^*(U^* - c^*)\tilde{v}_x^* + \rho \mathrm{d}_r^* U^* \tilde{v}_r^* = -\mathrm{i}k\tilde{p}^* + \mu(\mathrm{d}_r^{*2} + r^{*-1}\mathrm{d}_r^* - k^{*2})\tilde{v}_x^*, \tag{A 14}$$

$$\rho \mathrm{i}k^*(U^* - c^*)\tilde{v}_r^* = -\mathrm{d}_r^*\tilde{p}_f^* + \mu(\mathrm{d}_r^{*2} + r^{*-1}\mathrm{d}_r^* - r^{*2} - k^{*2})\tilde{v}_r^*. \tag{A 15}$$

Using the scaled variable η, the continuity equation takes the form

$$-\mathrm{d}_\eta \tilde{v}_r^* + \mathrm{i}\tilde{v}_x^* = 0. \tag{A 16}$$

The dimensional base flow velocity profile is given by $U^* = \overline{V}U$, where $\overline{V}$ is the characteristic dimensional velocity of the base flow, and U is the non-dimensional functional form of the profile. Very near the interface, the dimensional base velocity can be expanded as

$$U^* = \overline{V}\ [U|_{r=1} + U'|_{r=1}(1 - r^*/R) + \cdots]. \tag{A 17}$$

Using the fact that $U|_{r=1} = 0$ and expressing r^*/R in terms of the variable η defined above, we have

$$U^* = (k^{-1}\overline{V})U'|_{r=1}\ \eta. \tag{A 18}$$

From this, it can be seen that in limit of high k, the appropriate velocity scale is $k^{-1}\overline{V}$, and consequently the pressure scale is $\rho k^{-2}\overline{V}^2$. In this limit, the appropriate scale for the dimensional wave speed c^* is also $k^{-1}\overline{V}$, and we define $c = c^*/(k^{-1}\overline{V})$. Using these scales to non-dimensionalize the x-momentum equation, we have, to leading order in k,

$$\mathrm{i}(U'|_{r=1}\eta - c)\tilde{v}_x + U'\tilde{v}_r = -\mathrm{i}\tilde{p}_f + \frac{\mu k^2}{\rho\overline{V}R}(\mathrm{d}_\eta^2 - 1)\tilde{v}_x. \tag{A 19}$$

For the case of inviscid modes, we consider $\mu k^2/(\rho\overline{V}R) \gg 1$. The r-momentum equation can be scaled similarly and we obtain

$$\mathrm{i}(U'|_{r=1}\eta - c)\tilde{v}_r = \mathrm{d}_\eta\tilde{p}_f + \frac{\mu k^2}{\rho\overline{V}R}(\mathrm{d}_\eta^2 - 1)\tilde{v}_r. \tag{A 20}$$

The dimensional normal velocity continuity at $r = 1$ is given by $\tilde{v}_r^* = -\mathrm{i}k^*c^*\tilde{u}_r^*$. Using the scaling for $\tilde{v}_r^*$, c^* and k^* in this equation, we can obtain the scale for $\tilde{u}_r^*$ and this turns out to be $\tilde{u}_r^* = (k^{-1}R)\tilde{u}_r$. From the mass conservation equation for the wall medium, we also have $\tilde{u}_x^* = (k^{-1}R)\tilde{u}_x$. The pressure in the wall medium is scaled with the same scale as the fluid pressure, i.e. $\rho k^{-2}\overline{V}^2$. The dimensional x-momentum balance in the wall medium is given by

$$-k^{*2}c^{*2}\rho\tilde{u}_x^* = -\mathrm{i}k^*\tilde{p}_g^* + G(\mathrm{d}_r^{*2} + (r^*)^{-1}\mathrm{d}_r^* - k^{*2})\tilde{u}_x^*. \tag{A 21}$$

Using the scalings for $k^*, c^*, \tilde{u}_x^*, \tilde{p}_g^*$ in (A 21), we obtain

$$-c^2\tilde{u}_x = -\mathrm{i}\tilde{p}_g + \frac{Gk^2}{\rho\overline{V}^2}(\mathrm{d}_\eta^2 - 1)\tilde{u}_x. \tag{A 22}$$

The elastic stresses in the wall medium will be of the same order as the inertial stresses when $Gk^2/\rho\overline{V}^2 \sim O(1)$. This implies that $(k/\Gamma)^2 \sim O(1)$, and hence $\Gamma \sim k$. Therefore, for a fixed Σ, the Reynolds number for the modes analysed in this paper scales as

$Re = \Sigma^{1/2}\Gamma$, i.e. $Re \sim k$ in the limit of $k \gg 1$. To summarize, in the limit of low k, the scaling relation is $Re \sim k^{-1}$ and in the limit of high k, $Re \sim k$. Consequently, the critical Reynolds number occurs at $k \sim O(1)$. We conclude that the scalings of both the upper and lower branches for singular inviscid modes in a flexible tube are completely different from the conventional scalings of Tollmien–Schlichting modes for developing flow in a rigid tube. Therefore, the present modes are not a perturbation of the already known branches for the stability of developing flow in a rigid tube.

REFERENCES

Benjamin, T. B. 1960 Effect of a flexible surface on boundary layer stability. *J. Fluid. Mech* **9**, 513–532.

Carpenter, P. W. & Gajjar, J. S. B. 1990 A general theory for two and three dimensional wall-mode instabilities in boundary layers over isotropic and anisotropic compliant walls. *Theoret. Comput. Fluid Dyn.* **1**, 349–378.

Carpenter, P. W. & Garrad, A. D. 1985 The hydrodynamic stability of flows over Kramer-type compliant surfaces. Part 1. Tollmien–Schlichting instabilities. *J. Fluid. Mech* **155**, 465–510.

Carpenter, P. W. & Garrad, A. D. 1986 The hydrodynamic stability of flows over Kramer-type compliant surfaces. Part 2. flow induced surface instabilities. *J. Fluid. Mech* **170**, 199–232.

Davies, C. & Carpenter, P. W. 1997 Instabilities in a plane channel flow between compliant walls. *J. Fluid. Mech.* **352**, 205–243.

Drazin, P. & Reid, W. 1981 *Hydrodynamic Stability*. Cambridge University Press.

Duncan, W., Thom, A. S. & Young, A. 1960 *An Elementary Treatise on the Mechanics of Fluids*. Edward Arnold (Publishers) Ltd., London.

Eagles, P. M. & Smith, F. 1980 The influence of nonparallelism in channel flow stability. *J. Engng Maths* **14**, 219–237.

Eagles, P. M. & Weissman, M. 1975 On the stability of slowly varying flow: the divergent channel. *J. Fluid. Mech.* **69**, 241–262.

Garg, V. K. 1981 Stability of developing flow in a pipe: non-axisymmetric disturbances. *J. Fluid Mech.* **110**, 209–216.

Gaster, M. 1972 On the effects of boundary layer growth on flow stability. *J. Fluid. Mech.* **66**, 465–480.

Govindarajan, R. & Narasimha, R. 1997 A low-order theory for stability of non-parallel boundary-layer flows. *Proc. R. Soc. Lond.* A **453**, 2537–2549.

Hornbeck, R. W. 1963 Laminar flow in the entrance region of a pipe. *App. Sci. Res.* **110**, 224–232.

Krindel, P. & Silberberg, A. 1979 Flow through gel-walled tubes. *J. Colloid Interface Sci.* **71**, 34–50.

Kumaran, V. 1995*a* Stability of the viscous flow of a fluid through a flexible tube. *J. Fluid. Mech.* **294**, 259–281.

Kumaran, V. 1995*b* Stability of the flow of a fluid through a flexible tube at high Reynolds number. *J. Fluid. Mech* **302**, 117–139.

Kumaran, V. 1996 Stability of an inviscid flow through a flexible tube. *J. Fluid. Mech* **320**, 1–17.

Kumaran, V. 1998*a* Asymptotic analysis of wall modes in a flexible tube. *Eur. Phys. J.* B **4**, 519–527.

Kumaran, V. 1998*b* Stability of fluid flow through a flexible tube at intermediate Reynolds number. *J. Fluid. Mech* **357**, 123–140.

Kumaran, V. 1998*c* Stability of wall modes in a flexible tube. *J. Fluid. Mech* **362**, 1–15.

Kumaran, V., Fredrickson, G. H. & Pincus, P. 1994 Flow induced instability of the interface between a fluid and a gel at low Reynolds number. *J. Phys. Paris* II **4**, 893–904.

Kumaran, V. & Srivatsan, L. 1998 Stability of fluid flow past a membrane. *Eur. Phys. J.* B **2**, 259–266.

Lahav, J., Eliezer, N. & Silberberg, A. 1973 Gel-walled cylindrical channels as models for microcirculation: Dynamics of flow. *Biorheology* **10**, 595–604.

Landahl, M. T. 1962 On the stability of a laminar incompressible boundary layer over a flexible surface. *J. Fluid. Mech* **13**, 609–632.

LaRose, P. G. & Grotberg, J. B. 1997 Flutter and long-wave instabilities in compliant channels conveying developing flows. *J. Fluid. Mech.* **331**, 37–58.

Silberberg, A. 1987 Physico-chemical Hydrodynamics in turbulent flows close to an interface. *Physico-chem. Hydrodyn.* **9**, 419–426.

Smith, F. & Bodonyi, P. M. 1980 On the stability of the developing flow in a channel or circular pipe. *Q. J. Mech. Appl. Maths* **33**, 293–320.

Srivatsan, L. & Kumaran, V. 1997 Stability of the interface between a fluid and gel. *J. Phys. Paris* II **7**, 947–963.

Sutterby, J. L. 1965 Finite difference analysis of viscous laminar converging flow in conical tubes. *App. Sci. Res.* A **15**, 241–252.

Tritton, D. 1977 *Physical Fluid Dynamics*. Van Nostrand Reinhold Company.